Applied Geochemistry 137 (2022) 105197

Contents lists available at ScienceDirect

Applied Geochemistry

journal homepage: www.elsevier.com/locate/apgeochem

Nickel retention by calcium silicate hydrate phases: Evaluation of the role of the Ca/Si ratio on adsorption and precipitation processes

Tiziana Missana *, Miguel García-Gutiérrez, Ursula Alonso, Oscar Almendros-Ginestá

CIEMAT, Physical Chemistry of Actinides and Fission Products Unit, Department of Environment, Avenida Complutense 40, 28040, Madrid, Spain

ARTICLE INFO

Editorial handling by Dr D A. Kulik

Keywords:
Adsorption
Surface precipitation
Surface complexation modelling
Radioactive waste

ABSTRACT

The objective of the present study is to investigate Ni retention processes in Calcium Silicate Hydrate (CSH) phases, as the main cement hydration products, and to describe them in a generalized form for the first time. In particular, the effects of the CSH Ca/Si ratio (from 0.8 to 1.6) on the equilibrium water chemistry, Ni speciation, adsorption and solubility have been addressed. Nickel adsorption tends to decrease as the Ca/Si ratio increases, especially when Ca/Si is < 1.2, and then Ca/Si becomes less relevant. The *"adsorption"* region is limited to low final aqueous Ni concentrations ($<5{\cdot}10^{-9}$ M), and when the Ni concentration exceeds this limit, an increase in the (apparent) distribution coefficient, K_d, is observed, which is related to precipitation processes. The onset of precipitation depends on Ni solubility but also on the Ca/Si ratio: at the lowest ratio, the lowest Ni concentration occurs when the apparent K_d starts to increase. The existence of Ni–Si phases as surface precipitates could explain the observed experimental behaviour, which is not totally explicable assuming $Ni(OH)_2(s)$ as the unique phase limiting Ni solubility. Nickel retention on the CSH phases was analysed and interpreted with the help of surface complexation modelling using an electrostatic double layer approach and accounting for the major species present in solution for each CSH. The uncertainties in the available Ni thermodynamic database under alkaline conditions and in the presence of Si are underlined.

1. Introduction

To ensure the effective and long-term confinement of hazardous elements as radionuclides (RNs), deep knowledge of their interactions with barrier materials is required. All factors affecting RN aqueous speciation, solubility, and interactions with surrounding solids are relevant to predict migration patterns. A fundamental understanding of RN environmental behaviour is needed to assess the long-term safety of radioactive waste disposal, support management decisions and minimise the associated risks (Payne et al., 2013).

Nickel radioactive isotopes (^{59}Ni and ^{63}Ni) can be formed by neutron activation in nuclear facilities; they are critical RNs that can be found in low- or intermediate-level radioactive waste (LILRW) following the decommissioning of metallic materials (Carboneau and Adams, 1995).

In LILRW disposal, cements are typical containment/conditioning materials (Grambow et al., 2020), and Calcium Silicate Hydrate (CSH) phases are among the main mineral components in cements (Lothenbach and Nonat, 2015); they are considered important sorbents because of their high specific surface area (Roosz et al., 2016).

The mechanisms of radioactive Ni retention under hyperalkaline conditions generated by cementitious materials are still unclear and debated. The most recent review of RN sorption data for cementitious materials (Ochs et al., 2015) indicated that Ni has been a largely studied RN in the framework of LILRW disposal; nevertheless, published results concerning Ni retention by CSH phases are scarce and sometimes controversial.

Discrepancies observed for Ni adsorption data corresponding to CSH phases can be related to different causes, such as experimental difficulties and/or lack of up-to-date reliable thermodynamic data. For example, the complications in differentiating adsorption from precipitation, due to the low Ni solubility under cementitious conditions, and/or the existing uncertainties in $Ni(OH)_2$ solubility (González-Siso et al., 2018) contribute to inappropriate data analysis. Sometimes, experimental problems related to the use of liquid phases, mimicking cement water(s), but not in real equilibrium with the CSH phases, may also have mistaken the interpretation of the results.

Regarding the dependence of Ni sorption on the Ca/Si ratio, Noshita et al. (2001) did not observe any, whereas Aggarwal et al. (2000)

* Corresponding author.
E-mail address: tiziana.missana@ciemat.es (T. Missana).

https://doi.org/10.1016/j.apgeochem.2022.105197
Received 15 August 2021; Received in revised form 13 December 2021; Accepted 3 January 2022
Available online 5 January 2022

reported variation in the distribution coefficients with the Ca/Si ratio. As a principal consequence, different interpretations of Ni retention were provided as follows: in the first case, the interaction of Ni with CSH phases was thought to be no electrostatic, and $Ni(OH)_2(aq)$ adsorption was assumed; however, in the latter case, Ni–Ca exchange was considered the main retention mechanism.

Indeed, the role of the Ca/Si ratio on Ni retention in CSH phases is still an open point, but other knowledge gaps on its retention mechanisms still exist. Furthermore, very few attempts have been made to describe Ni retention on CSH phases by means of (quasi-) mechanistic adsorption models, as the existence of some uncertainties in Ni thermodynamic data at high pH also boosts the disparity in data interpretation.

At present, the most important revision of Ni thermodynamic data is the one from Gamsjäger et al. (2005) (OECD-NEA thermodynamic database, TDB). Recently, González-Siso et al. (2018) argued on the possible incorrectness of some of the constants suggested in this TDB, particularly in relation to the solubility of $Ni(OH)_2(s)$ and on the formation of the anionic species $Ni(OH)_3^-$ under hyperalkaline conditions.

The following two main goals are set in this work: 1) to understand the dependence of Ni retention on the Ca/Si ratio of CSH, including adsorption and precipitation processes, and 2) to develop a sorption model able to reproduce the retention behaviour of Ni on CSH phases under a wide range of conditions (CSH Ca/Si ratio and Ni concentration) after thermodynamic Ni database revision.

A large set of experimental data was necessary for gathering information on Ni adsorption behaviour at different Ca/Si ratios (from 0.8 to 1.6), and to analyse Ni precipitation behaviour, the range of concentrations in the isotherms was extended above the solubility limit. Ni sorption isotherms were also carried out on nanocrystalline silica and SiO_2 and on portlandite, $Ca(OH)_2$, as the endmembers of CSH phases (Lothenbach and Nonat, 2015), especially focusing on Ni precipitation behaviour in both materials.

Nickel retention on the CSH at different Ca/Si ratios was interpreted with the help of thermodynamic modelling. An electrostatic double layer approach has been adopted, previously developed to study cation (Missana et al., 2017, 2018) and anion (Missana et al., 2019) retention on the CSH phases. As modelling fundamental input, the available Ni thermodynamic data were revised.

Ni precipitation is triggered at the lowest concentration at the lowest Ca/Si ratio, and this behaviour does not seem to be in agreement with the existence of the unique solubility limiting phase, $Ni(OH)_2(s)$. Ni retention model could be improved including both the formation of surface precipitates and the contribution of Si to Ni surface precipitation, considering the conceptual approach of surface precipitation proposed by Farley et al. (1985).

2. Materials and methods

2.1. Solid phases

The CSH phases (10 g L^{-1}) were prepared with different CaO/SiO_2 (Ca/Si) molar ratios, from 0.8 to 1.6. The method used was the "*direct*" method reported in different papers (Pointeau, 2000; Missana et al., 2017), which basically consists of mixing CaO (Aldrich, 99.9% purity CAS 1305–78–8) and SiO_2 (Aldrich 99,8% purity CAS 7631–86–9) at the requested molar ratio in ultrapure water, previously boiled and flushed with N_2 to minimise CO_2 contamination. The suspensions were prepared and stored in HDPE dark bottles in a glovebox under N_2 atmosphere, and they were aged for approximately 1 month. The synthesis of the CSH gels is considered completed when the pH and conductivity of the suspensions (checked daily) reach constant values.

Part of the suspensions was filtered through 100 nm Millipore filters. The supernatants were analysed to determine aqueous Ca and Si (by ICP-OES with a VARIAN 735 ES spectrometer); the rest was stored for diluting the initial suspensions when required. Their surface area was determined by N_2-BET.

Sorption tests were also carried out with SiO_2 (Aldrich 99,8% purity, BET = 175–225 m^2 g^{-1}) and portlandite obtained after dissolution/recrystallisation of $Ca(OH)_2$ (Merck, CAS: 1305–62–0). The BET of the portlandite is 13.5 m^2 g^{-1}.

The adsorbents were analysed by attenuated total reflection-Fourier transform infrared (ATR-FTIR) spectroscopy, scanning electron microscopy (SEM) and energy dispersive X-ray spectroscopy (EDS) to check that the synthesis was correct. The ζ-potential of the suspensions was measured by laser Doppler electrophoresis using a Malvern Zetamaster apparatus equipped with a 5-mW He–Ne laser (λ = 633 nm and scattering angle 90°). For electrophoretic measurements, the suspensions were diluted to 1 g/L with their own equilibrium water, previously separated by filtering.

2.2. Radionuclide

The radionuclide used for this study was ^{63}Ni, supplied by Eckert & Ziegler Isotope Products. Ni is in the form of $NiCl_2$ in HCl 0.1 M without carrier. In sorption isotherms, to reach Ni concentrations higher than $1{\cdot}10^{-8}$ M, stable Ni ($NiCl_2$, Merck) was added. ^{63}Ni has a half-life of 100.1 years and undergoes radioactive decay by β^- emission. Its activity in solution was measured with a liquid scintillation analyser Tri-Carb 4910 TR (Perkin Elmer) and using Ultima Gold™ as a scintillation cocktail. The uncertainty for the counting procedure is less than 2%. The detection limit is approximately $5{\cdot}10^{-12}$ M.

2.3. Batch sorption experiments

Batch sorption experiments were carried out at a temperature of 22 ± 2 °C within a glove box under a N_2 atmosphere. The CSH suspensions were used as prepared (10 g L^{-1}) or diluted to 1 g L^{-1}. Sorption isotherms were carried out with [Ni] concentrations from approximately $5{\cdot}10^{-10}$ M to $5{\cdot}10^{-4}$ M with CSH at different Ca/Si ratios. The kinetic of the sorption process was investigated first to evaluate the time required for the attainment of sorption equilibrium. The contact time selected for performing the isotherms was 7–15 days.

After the contact time, the solid and liquid phases were separated by centrifugation (21255 g, 30 min) with a JOUAN MR23i centrifuge. Three aliquots of the supernatant were extracted from each tube for the analysis of the final Ni activity.

Considering the range of Ni concentrations analysed in the isotherms, not only adsorption but also precipitation is expected; thus, the measured distribution coefficients will be defined as "apparent" (K_d*(app)*, mL·g^{-1}) because they consider the concentration of both adsorbed and/or precipitated Ni ($[Ni]_{solid}$):

$$K_d(app) = \frac{[Ni]solid}{[Ni]eq} \cdot \frac{V}{m} \quad \text{E.1}$$

As in the usual K_d definition, $[Ni]_{eq}$ represents the Ni remaining in the aqueous phase at equilibrium, *m* is the mass of the solid [g] and *V* is the volume of the solution [mL].

Sorption experiments with SiO_2 and portlandite were carried out with a solid-to-liquid ratio of 1 g L^{-1}; SiO_2 was suspended in NaOH (pH = 9.5), and portlandite was suspended in its equilibrium water (pH = 12.56, [Ca]~20 mM).

2.4. Modelling description

A simplified description of the CSH surface characteristics based on a classical diffuse double layer (DDL) approach was used, and more details can be found in Missana et al. (2017). In summary, the model contemplates the existence of two different types of silanol (SiOH) sites at the CSH surface (*strong*, S and *weak*, W) and exchange sites (CaX_2) initially occupied by Ca.

Under the alkaline conditions considered for the CSH phases, the

silanol-like sites are deprotonated, according to the following reaction:

$$SiOH \leftrightarrow SiO^- + H^+ \quad \text{E.2}$$

The model considers calcium as an ion determining the potential (IDP); thus, the following reaction between the deprotonated weak silanol-like groups and Ca is of interest:

$$SiO^- + Ca^{2+} \leftrightarrow SiOCa^+ \quad \text{E.3}$$

In the CSH phases, cation (M^{z+}) surface complexation can be expressed by reactions of the following type:

$$SiOH + M^{z+} \leftrightarrow SiOM^{z-1} + H^+ \quad \text{E.4}$$

And ion exchange with divalent ions (as Ni) as:

$$X_2Ca + M^{2+} \leftrightarrow X_2M + Ca^{2+} \quad \text{E.5}$$

Finally, anion adsorption is also possible on CSH through the formation of surface complexes with silanol-like surface sites where Ca^{2+} is already adsorbed as follows:

$$SiOCa^+ + An^{n-} \leftrightarrow SiOCaAn^{(n-1)-} \quad \text{E.6}$$

The surface parameters needed for modelling the CSH surface properties are summarised in Table 1. Model calculations were performed using the geochemical CHESS v 2.4 code (Van der Lee and de Windt, 1999).

3. Results and discussion

3.1. CSH characterisation

The CSH phases were prepared at five different Ca/Si ratios from 0.8 to 1.6 and labelled CSH(Ca/Si). Table 2 summarises the main characteristics of each phase. The pH of the suspensions and the aqueous Ca increase as the Ca/Si ratio increases, whereas the aqueous Si decreases. This is the first indication that the composition of the aqueous phase in equilibrium with the solids depends on the Ca/Si ratio and that Ni speciation and retention behaviour will not necessarily be the same in all the CSH phases.

Furthermore, the surface potential of the CSH phases depends on the aqueous Ca concentration and can be either negative or positive; thus, Ca is considered an ion determining the potential (IDP) of CSH phases, and the *point of zero charge* corresponds to an aqueous Ca concentration of 130–180 ppm (Ca/Si ratio between 1 and 1.2).

Therefore, the affinity for cations (and anions) for the CSH surface is expected to be somewhat dependent on the Ca/Si ratio.

Finally, the zetapotential of SiO_2 under the condition of sorption tests (pH 9.5) was negative (~−40 mV), whereas that of portlandite (pH 12.56) was positive (~+30 mV).

The BET (Brunauer–Emmett–Teller) surface area of the CSH phases, measured by N_2 adsorption, also depends on the Ca/Si ratio, which is generally higher when the Ca/Si is lower. The mean N_2-BET value for CSH phases with Ca/Si < 1.6 was 144 ± 40 $m^2\ g^{-1}$, comparable to that proposed by (Tits et al., 2006) of 148 $m^2\ g^{-1}$. However, the value measured in the CSH (1.6) was significantly lower (73 $m^2\ g^{-1}$). For model calculations, the mean value of 144 $m^2\ g^{-1}$ will be used if Ca/Si < 1.6, whereas for CSH (1.6), the measured value (73 $m^2\ g^{-1}$) will be considered.

Table 1
Reactions and parameters used to define the CSH surface for sorption modelling. (From Missana et al., 2017).

Description	Composition (CHESS code)	LogK
Silanol de-protonation (S and W sites)	$Si_{s,w}O^- = 1\ Si_{s,w}OH, -1\ H^+$	−6.80 ± 0.5
Exchange site (E)	X_2Ca	
Complexation of Ca (IDP)	$Si_wOCa^+ = 1\ Si_wOH, -1\ H^+, 1\ Ca^{2+}$	−4.12

The densities of W and S silanol sites are 13 and $3.5{\cdot}10^{-3}$ μmol m^{-2}, respectively, and the density of exchange sites is 2 μmol m^{-2}.

Table 2
Characteristics of the different CSH phases used in this study.

Sample	pH	Conductivity (μS·cm^{-1})	Ca (mg·L^{-1})	Si (mg·L^{-1})	ζ-potential (mV ± 5 mV)
CSH (0.8)	10.28 ± 0.13	187 ± 39	44 ± 5	71 ± 10	−16
CSH (1.0)	11.49 ± 0.12	1080 ± 116	96 ± 10	3.5 ± 0.5	−5
CSH (1.2)	11.95 ± 0.22	2340 ± 110	207 ± 16	1.5 ± 0.4	5
CSH (1.4)	12.15 ± 0.10	4760 ± 160	335 ± 7	0.45 ± 0.1	10
CSH (1.6)	12.36 ± 0.05	6170 ± 95	590 ± 36	0.14 ± 0.05	17

The characterisation of the solid by FTIR-ATR and SEM-EDS confirmed that the solids produced are CSH with the required Ca/Si ratio. The results of this characterisation are included in the Supplementary Material (FTIR-ATR spectra are included in Fig. S1, and an SEM image of the CSH (1.4) and the respective EDS spectrum is included in Fig. S2).

3.2. Batch sorption tests

Kinetic tests from 1 to 30 days were carried out (data in Supplementary Material, Fig. S3) to determine the contact time needed to reach equilibrium. The rest of the experiments detailed below were performed with a contact time between 7 and 15 days.

Fig. 1 shows the Ni sorption isotherms in five CSH phases (0.8, 1, 1.2, 1.4 and 1.6) expressed as logarithm of the apparent K_d as a function of the logarithm of Ni concentration at equilibrium in the aqueous phase (Log(Ni_{eq})).

The same data represented as the logarithm of the adsorbed element por unit of mass (Ni_{ads}, mol·g^{-1}) versus the logarithm of the Ni final aqueous concentration at the equilibrium (Ni_{eq}, M), are included in the Supplementary Material (Fig. 4S).

The experimental data can be divided into two different zones. The first is at a low Ni equilibrium concentration ([Ni_{eq}] < $1{\cdot}10^{-9}$ M), where K_d(app) remains constant within the experimental error and Ni is linearly adsorbed on the CSH surface.

In the second region, as the Ni concentration increases, the apparent

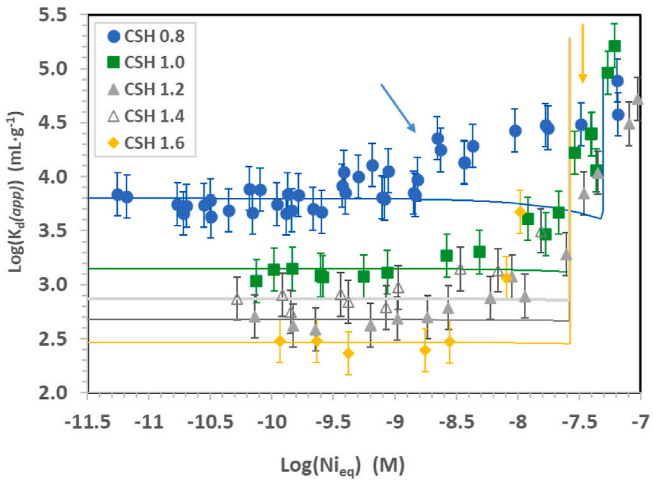

Fig. 1. Sorption isotherms of Ni on CSH at different Ca/Si ratios. Continuous lines correspond to the fit obtained with the parameters obtained for each CSH, summarised in Table 4.

K_d also increases, indicating the existence of Ni precipitation processes. The Log(K_d) values determined in the *adsorption zone* are approximately 3.8, 3.2 and 2.5 for CSH (0.8), CSH (1.0) and CSH (1.6), respectively, showing a decrease in adsorption as the Ca/Si ratio increases. The exception is represented by CSH(1.4), where the adsorption is slightly higher than that determined in CSH(1.2), an effect that, in principle, could be related to the variability range of measurements.

The largest difference in adsorption can be observed when the Ca/Si ratio increases from 0.8 to 1.0 (almost one order of magnitude), but for higher Ca/Si ratios, the differences are clearly smaller. This dependence is better explained in Fig. 2, which summarises the dependence of Log (K_d) on the Ca/Si ratio. Fig. 2 includes sorption values obtained at an initial Ni concentration [Ni] = $1{\cdot}10^{-9}$ - $5{\cdot}10^{-8}$ M (i.e., in the adsorption region) from the sorption isotherms and other single sorption tests.

From Ca/Si 0.8 to 1.2, the sorption decrease is more evident than for higher Ca/Si, where K_d values are much more similar. For Ca/Si < 1.2, the sign of the CSH surface potential is negative, and a greater affinity for cations is expected. For anions, the opposite is true.

Regarding Ni precipitation, the increase in the apparent K_d indicates the onset of precipitation processes. For the phases with higher Ca/Si, the K_d increase is sharp, whereas for CSH(0.8), the first increase observed (indicated with the blue arrow in the figure) is more gradual, suggesting the existence of other possible mechanisms, such as surface precipitation.

Thus, the aqueous chemistry (pH and Ca and Si concentrations) characteristics of the different CSH phases affect adsorption but may also have a role in the overall solubility of Ni.

3.3. NI speciation and sorption modelling

The Ni thermodynamic database initially used for calculation was the one compiled by the OECD-NEA (Gamsjäger et al., 2005), included in the ThermoChimie database (Giffaut et al., 2014) and summarised in Table 3.

Fig. 3 (a, b) shows Ni speciation as a function of pH (from 10 to 13) at two different Ni concentrations ($1{\cdot}10^{-9}$ M and $5{\cdot}10^{-7}$ M) calculated with these thermodynamic data. At low Ni concentrations ([Ni] = $1{\cdot}10^{-9}$ M, Fig. 3a), two predominant species exist in the entire pH range: neutral $Ni(OH)_2$ (aq) and negatively charged $Ni(OH)_3^-$. Positively charged Ni^{2+} and $NiOH^+$ are detectable only at pH < 11 and at a low concentration.

According to this TDB, the solid limiting Ni solubility, $Ni(OH)_2$(s), would precipitate at a Ni concentration above $1{\cdot}10^{-7}$ M, which is a concentration almost 2 orders of magnitude higher than the limit of precipitation experimentally seen in sorption isotherms (Fig. 1).

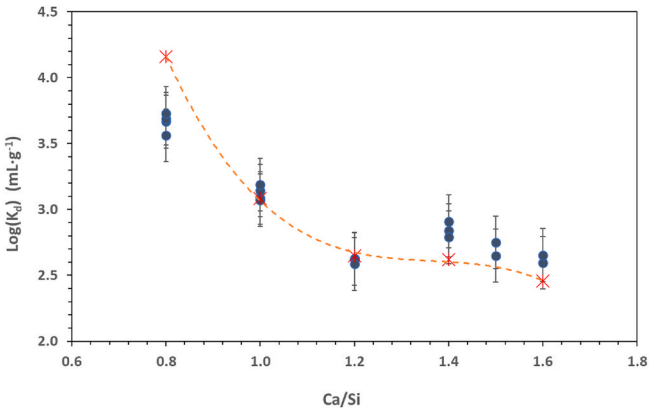

Fig. 2. Log(K_d) as a function of the CSH Ca/Si ratio. $[Ni]_{ini}$ = $1{\cdot}10^{-9}$ - $5{\cdot}10^{-8}$ M. Red stars correspond to the values calculated with the mean values of the parameters of Table 4. (For interpretation of the references to colour in this figure legend, the reader is referred to the Web version of this article.)

Table 3
Thermodynamic data for the calculation of Ni speciation. Bold: corrected values as suggested by Gonzalez-Siso et al. (2018). The species indicated with (*) was recalculated in this work.

Species	Composition (CHESS code)	OECD-NEA TDB (Gamsjäger et al., 2005).	Values used in this work
Ni(OH) [+]	1 Ni[2+], −1 H[+], 1 H_2O	−9.54	−9.54
$Ni(OH)_2$ (aq)	1 Ni[2+], −2 H[+], 2 H_2O	−18.00	**−19.7**
$Ni(OH)_3$ [-]	1 Ni[2+], −3 H[+], 3 H_2O	−29.38	**−33.3 (*)**
$Ni_2(OH)$ [3+]	2 Ni[2+], −1 H[+], 1 H_2O	−10.60	−10.60
$Ni_4(OH)_4$ [4+]	4 Ni[2+], −4 H[+], 4 H_2O	−27.52	−27.52
$Ni(OH)_2$ (s)	1 Ni[2+], −2 H[+], 2 H_2O	−11.03	**−12.10**

Furthermore, as seen in the speciation diagram calculated for [Ni] = $5{\cdot}10^{-7}$ M (Fig. 3b), as the pH increases, the hydroxide dissolves, leading to a large increase in the negatively charged $Ni(OH)_3^-$.

González-Siso et al. (2018) performed solubility tests with Ni $(OH)_2$(s) and observed that the solubility of this solid is lower than that predicted by the most updated Ni thermodynamic database (Gamsjäger et al., 2005) and that redissolution of $Ni(OH)_2$(s) was not observed up to pH 13, suggesting that, at least up to this pH, $Ni(OH)_3^-$ cannot be a predominant species in solution. Therefore, they suggested excluding Ni $(OH)_3^-$ from the database. However, this might be an arbitrary decision pursuant to the detection limit of the experiments. For this reason, we accounted for their Ni solubility data, obtained under relevant conditions for the cementitious environment, to determine a (limit) value for $Ni(OH)_3^-$ formation.

The results of the calculations are shown in the Supplementary Material (Fig. 5S). Considering their results, this constant cannot be higher than −32, and a value of −33.3, which reproduces their data satisfactorily, was selected.

Thus, the Ni thermodynamic constants used for the modelling are those summarised in the last column of Table 3, considering Ni TDB (Gamsjäger et al., 2005), the revised value of $Ni(OH)_2$(s) solubility (González-Siso et al., 2018) and the present estimate for the formation constant of $Ni(OH)_3^-$. The speciation diagram obtained with these corrected data under the same conditions of previous calculations is shown in Fig. 3 (c and d). At low Ni concentrations ([Ni] = $1{\cdot}10^{-9}$ M, Fig. 3c), neutral $Ni(OH)_2$ (aq) is predominant in almost the entire pH region, but as a neutral species, it is not considered to contribute to adsorption. Other aqueous species present in non-negligible concentrations are cationic Ni^{2+} and $Ni(OH)^+$ (up to pH 11 and 12, respectively). Negatively charged $Ni(OH)_3^-$ starts to appear at pH > 11.5.

The analysis of Ni speciation is fundamental for understanding its adsorption and solubility in the different CSH phases because if the relative concentration of the species varies with pH, their contribution to adsorption in the different CSH phases is different.

Therefore, for CSH(0.8) (pH = 10.28), the main species will be positively charged $Ni(OH)^+$ and Ni^{2+}; for CSH(1.0), CSH(1.2) and CSH (1.4) (pH = 11.49, 11.95 and 12.15), all charged species are at very low concentrations, but with a slight predominance of $Ni(OH)^+$ or $Ni(OH)_3^-$. Finally, for the positively charged CSH(1.6) (pH = 12.36), the main adsorbing species to be considered is anionic $Ni(OH)_3^-$. This means that the possible co-adsorption of cationic and anionic species might occur, and this possibility must be accounted for (Missana et al., 2019).

At [Ni] = $5{\cdot}10^{-7}$ M, above the Ni solubility limit (Fig. 3d), Ni $(OH)_2$(s) is predicted to be the only solid limiting solubility over the entire range of pH values analysed. Neutral $Ni(OH)_2$(aq) is present in all pH ranges; Ni^{2+} and $Ni(OH)^+$ are present at very low concentrations, appreciable only for pH < 11, and $Ni(OH)_3^-$ is seen only at pH > 12.

Table 4
Surface complexes and definition according to the CHESS code and parameters used for the modelling of adsorption data. (*) From Missana et al. (2017).

	Complexes and Log(K)			
	X_2Ni 1 X_2Ca, −1 Ca^{2+}, 1 Ni^{2+}	$SiONi^+$ 1 SiOH, −1 H^+, 1 Ni^{2+}	$SiONiOH$ 1 SiOH, −2 H^+, 1 Ni^{2+}, 1 H_2O	$SiOCaNi(OH)_3$ 1 SiOH, −4 H^+, 1 Ni^{2+}, 1 Ca^{2+}, 3 H_2O
CSH(0.8)	1.3	−0.3	−9.05	−30.50
CSH(1.0)	1.3	−0.3	−8.60	−30.50
CSH(1.2)	1.3	−0.3	−8.60	−30.50
CSH(1.4)	1.3	−0.3	−8.50	−30.10
CSH(1.6)	1.3	−0.3	−8.60	−30.40
Mean	1.3(*)	−0.3(*)	**−8.67**	**−30.40**
St. Dev.	–	–	**0.22**	**0.17**

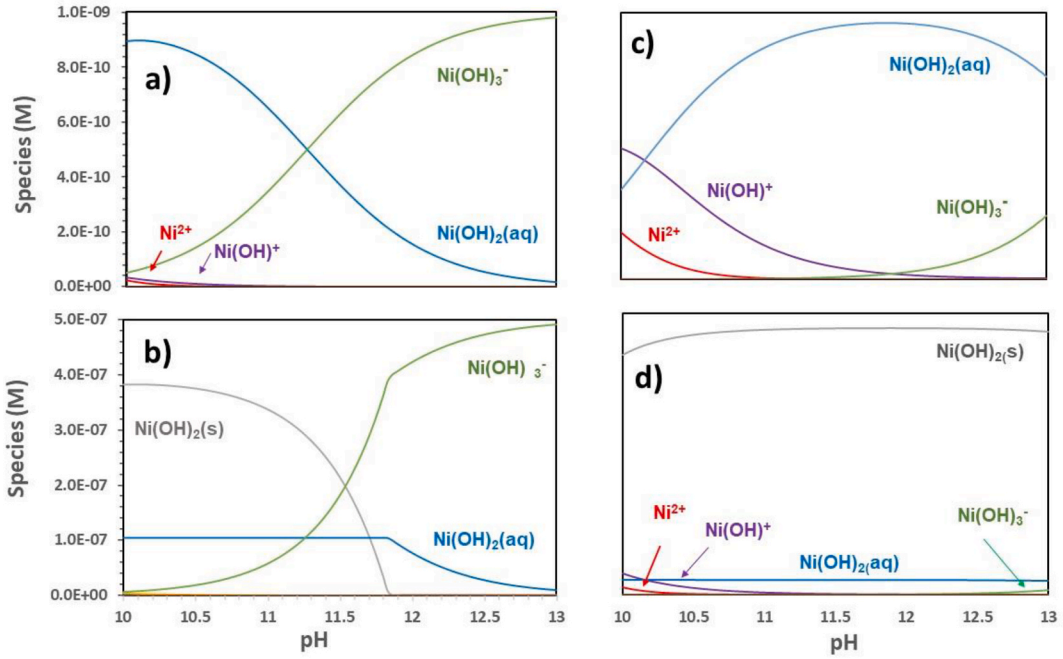

Fig. 3. Ni speciation (in $NaClO_4$ 0.1 M) with values in Table 2 a) and b) Thermodynamic data from Gamsjäger et al. (2005). c) and d) revised thermodynamic database. a) and c) [Ni] = $1{\cdot}10^{-9}$ M; b) and d) [Ni] = $5{\cdot}10^{-7}$ M.

Furthermore, with the revised thermodynamic constants, $Ni(OH)_2(s)$ precipitation agrees with the experimental study by Gonzalez-Siso et al. (2018) and occurs at a concentration approximately one order of magnitude lower than that predicted with the values of Gamsjäger et al. (2005).

Considering the calculations and the Ni speciation obtained (Fig. 3c and d, respectively), the following reactions were assumed for the formation of surface complexes, considering the possible adsorption of both cationic and anionic Ni species:

1) $X_2Ca + Ni^{2+} \leftrightarrow X_2Ni + Ca^{2+}$ *Ni–Ca cation exchange*
2) $SiOH + Ni^{2+} \leftrightarrow SiONi^+ + H^+$ *surface complexation of* Ni^{2+}
3) $SiOH + Ni(OH)^+ \leftrightarrow SiONiOH + H^+$ *surface complexation of* $Ni(OH)^+$
4) $SiOCa^+ + Ni(OH)_3^- \leftrightarrow SiOCaNi(OH)_3$ *surface complexation of* $Ni(OH)_3^-$

The surface reactions are summarised in Table 4, according to the nomenclature of the CHESS code. Ni adsorption was observed only at low Ni concentrations (Fig. 1); accordingly, Ni surface complexation was only considered on strong surface sites. In the calculations, Ni precipitation is allowed.

For reactions 1) and 2), the same constants used by Missana et al. (2017) for Ba^{2+} were taken and fixed for all CSHs. As observed in the speciation diagrams (Fig. 3c), Ni^{2+} is always a minor species in the alkaline range of interest and does not affect appreciable retention in CSH phases with Ca/Si > 0.8.

The best fit parameters obtained considering reactions 3) and 4) for each CSH are summarised in Table 4. The estimated constants for the surface complexation of $Ni(OH)^+$ and $Ni(OH)_3^-$ are very similar for all the CSH phases, with a standard deviation of approximately ±0.2. The results of modelling calculations for sorption isotherms are superimposed as continuous lines on the experimental data in Fig. 1.

The model allows predicting Ni adsorption in all the CSH phases analysed in this work in a quite satisfactory way. Calculations performed using the mean values of the constants obtained, also indicated in Table 4, reproduce very well the behaviour of adsorption as a function of the Ca/Si ratio (Fig. 2), with the only exception of CSH(0.8), where the model (red stars) overpredicts Ni adsorption by almost half an order of magnitude. In the calculated curve, CSH(1.4) represents an inflexion point in adsorption, and it is noticed that for Ca/Si ratios >1.2, the effect of the Ca/Si ratio becomes almost insignificant within the experimental error.

Upon the analysis of Ni adsorption, it is worth opening a discussion on the precipitation behaviour observed. The beginning of $Ni(OH)_2(s)$ precipitation is predicted when the aqueous Ni concentration exceeds 2–$5{\cdot}10^{-8}$ M. When this solubility limit is exceeded, $Ni(OH)_2(s)$ precipitation promotes a sharp increase in apparent K_d values; in the model, precipitation is revealed by a vertical line (yellow arrow, Fig. 1). However, especially in CSH (0.8), K_d gradually starts increasing at a Ni

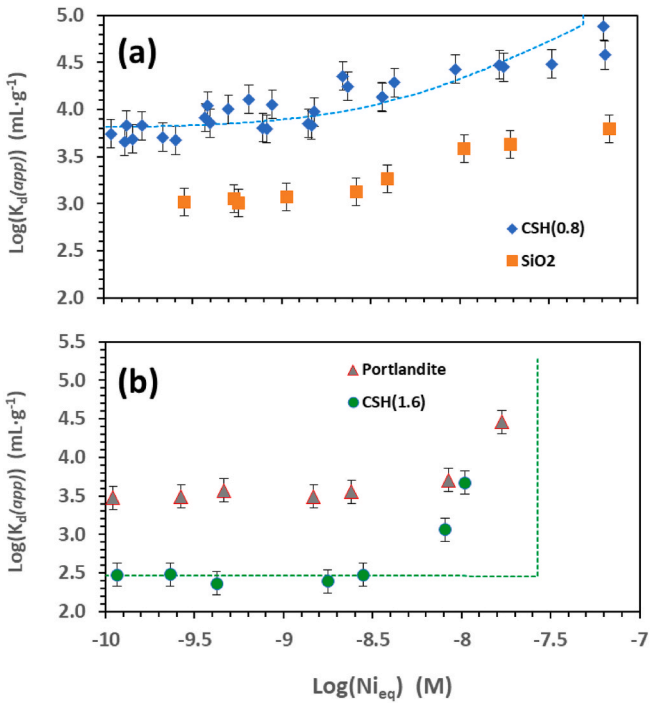

Fig. 4. Comparison of the Ni sorption isotherms on a) CSH(0.8) and SiO_2 and b) CSH(1.6) and portlandite. Attention is focused on the different precipitation behaviours. The lines, indicating different possible precipitation processes, are drawn to guide the eye.

concentration well below that predicted for $Ni(OH)_2(s)$ precipitation.

Ni retention in this intermediate region between the adsorption zone and the precipitation of $Ni(OH)_2(s)$ cannot be perfectly reproduced by the present adsorption/$Ni(OH)_2(s)$ precipitation model. From the experimental data, it seems that precipitation is somehow facilitated when the Ca/Si ratio is low, suggesting that Si may play a role in this process and in the overall Ni solubility.

To check this, Ni sorption isotherms were also carried out in SiO_2 and portlandite (Fig. 4), with the aim of focusing on the precipitation behaviour in both cases. Fig. 4a shows the sorption isotherms of Ni in SiO_2 compared with that of CSH(0.8), and Fig. 4b shows the sorption isotherm of Ni in portlandite compared to that of CSH (1.6).

Even if the objective of the present work is not to model Ni adsorption mechanisms on SiO_2 and portlandite, because more experimental data are still needed (i.e. surface sites density for both oxides) some comments on the results are due. In the case of SiO_2 (pH 9.5), according to the speciation diagram (Fig. 3c and d), the main Ni sorbing species will be the positively charged $Ni(OH)^+$ and Ni^{2+}, which can be directly complexed by the deprotonated silanol groups (SiO^-). In respect to the CSH phases, a slightly smaller adsorption capacity is observed (Fig. 4a), that can be explained by the absence of the Ni–Ca exchange adsorption mechanism in the oxide. In the case of portlandite, as occurs for the CSH (1.6), the main Ni adsorbing species is the anionic $Ni(OH)_3^-$. The concentration of this anionic species increases almost twice from pH 12.36 (CSH(1.6)) to 12.56 (portlandite) (Fig. 3c and d), and this can be the main reason why, portlandite is observed to adsorb more Ni than CSH (1.6) (Fig. 4b), together with the higher positive charge of the oxide.

Coming back to the focus (Ni precipitation behaviour) it is interesting to note that, in effect, Ni shows a similar precipitation behaviour in SiO_2 and CSH(0.8), i.e., much *smoother* than that observed in CSH (1.6) and portlandite, reinforcing the hypothesis on the potential role of Si in surface precipitation.

The smooth apparent K_d increase cannot be reproduced by modulating the solubility constants of $Ni(OH)_2(s)$ or considering any other solid limiting Ni solubility. Thus, for explaining Ni precipitation behaviour in the presence of CSH phases at a low Ca/Si ratio, the formation of surface precipitates is a plausible option.

Wieland and Van Loon (2002) and Wieland et al. (2006) suggested that in cements, Ni may form layered double hydroxides (LDHs) with a solubility lower than $Ni(OH)_2(s)$, and in particular, the formation of hydrotalcite-like layered double hydroxides (Ni–Al LDHs) was emphasised (Scheidegger et al., 2000).

Specific studies on Ni surface precipitation on the CSH phases are not available, but the formation of multinuclear surface complexes or Ni precipitates on the surface of silicates or clay minerals during sorption and under ambient environmental conditions has been reported for a long time (Charlet and Manceau, 1994; Nachtegaal and Sparks, 2002; Scheckel et al., 2000; Shi et al., 2012).

A surface precipitation process starts upon the adsorption of the metal, followed by homogeneous or heterogeneous surface nucleation and (crystalline) growth above the surface (Scheckel, 1998). Different approaches have been considered to describe surface precipitation (Farley et al., 1985; Degueldre and Kline, 2007), which have been mainly applied for oxyhydroxides and calcite (Comans et al., 1987). In their surface precipitation model (SPM), Farley et al. (1985) assumed that when a metal is adsorbed on a surface, a new surface phase is formed with the additional inclusion of aqueous ions (Fe, Ca, …) precipitating on the surface so that their composition varies between the original solid and the metal precipitate.

In the present system (Ni-CSH), two main processes should be accounted for the SPM: multilayer Ni^{2+} sorption on the surface and the formation of a solid solution between Ni and dissolved Si. Assuming such SPM to simulate the smooth increase of the apparent K_d is possible (dotted line in Fig. 4a). Nevertheless, in the absence of thermodynamic data on Ni–Si compounds, the solution is resolved but not unique, and the approach remains merely empirical and qualitative.

Even though the existence of different types of Ni–Si solids is reported in the literature, unfortunately, no reliable thermodynamic data are available for modelling calculations. Gamsjäger et al. (2005) discussed some studies about $Ni_2SiO_4(s)$, a nickel-olivine, concluding that its formation under ambient conditions is improbable and that, consequently, no studies on its formation in aqueous media exist. To the best of our knowledge, no other thermodynamic studies are available on the formation of Ni–Si solids under alkaline conditions.

Surely, more detailed studies on Ni solubility in the presence of Si/SiO_2 are necessary for a complete and unequivocal description of Ni retention in cementitious materials.

4. Conclusions

The retention of Ni on CSH phases with a Ca/Si ratio from 0.8 to 1.6 has been experimentally analysed, focusing on both adsorption and precipitation processes. Ni adsorption clearly depends on the Ca/Si ratio when it ranges from 0.8 to 1.2, with a clear decrease in sorption as the ratio increases. For Ca/Si > 1.2, the variation is much less evident, and the distribution coefficients are similar within the experimental error.

Ni adsorption could be successfully modelled in all Ca/Si ratios, considering a double layer approach with surface complexation of the species Ni^{2+}, $Ni(OH)_2^+$ and $Ni(OH)_3^-$ on strong silanol-like sites present at the CSH surface.

The adsorption zone for Ni is limited to quite a low equilibrium concentration ($[Ni_{eq}] < 5{\cdot}10^{-9}$ M); then, as the Ni concentration increases, the onset of precipitation processes is evidenced by the increase in the (apparent) K_d.

At the lowest Ca/Si ratio of 0.8 and in SiO_2, the increase in the apparent K_d is smooth and starts at a Ni aqueous concentration almost one order of magnitude smaller than the predicted $Ni(OH)_2(s)$ precipitation. Thus, the presence of Si seems to facilitate the formation of surface precipitates and a decrease in Ni overall solubility.

More detailed solubility studies of Ni in the presence of Si/SiO_2 under alkaline conditions would be desirable for an unequivocal

thermodynamic description of the system.

Geochemical and thermodynamic models are quite powerful tools to understand contaminant behaviour in complex systems, and their use can be extended to predict the impact of hazardous elements in different environmental fields.

Declaration of competing interest

The authors declare that they have no known competing financial interests or personal relationships that could have appeared to influence the work reported in this paper.

Acknowledgements

This study was partially supported by the European Union's Horizon 2020 Research and Innovation Programme under Grant Agreement no. 847593 (EURAD, CORI) and by the Spanish Ministry of Science and Innovation (PID2019–106398GB-I00, ARNO Project).

Appendix A. Supplementary data

Supplementary data to this article can be found online at https://doi.org/10.1016/j.apgeochem.2022.105197.

References

Aggarwal, S., Angus, M.J., Ketchen, J., 2000. Sorption of Radionuclides onto Specific Mineral Phases Present in Repository Cements. NSS/R312, AEA-D&R-0395, AEA technical Report.

Carboneau, M.L., Adams, J.P., 1995. Nickel-63. National Low-Level Waste Management Program Radionuclide Report Series, vol. 10. USA Department of Energy Report. DOE/LLW-126. https://inis.iaea.org/collection/NCLCollectionStore/_Public/26/054/26054999.pdf.

Charlet, L., Manceau, A., 1994. Evidence for the neoformation of clays upon sorption of Co(II) and Ni(II) on silicates. Geochem. Cosmochim. Acta 58, 2577–2582. https://doi.org/10.1016/0016-7037(94)90034-5.

Comans, R.N.J., Middelburc, J.J., 1987. Sorption of trace metals on calcite: applicability of the surface precipitation model. Geochem. Cosmochim. Acta 51, 2587–2591.

Degueldre, C., Kline, A., 2007. Study of thorium association and surface precipitation on colloids. Earth Planet Sci. Lett. 264 (1).

Farley, K.J., Dzombak, D.A., Morel, F.M.M., 1985. A surface precipitation model for the sorption of cations on metal oxides. J. Colloid Interface Sci. 106, 226–242. https://doi.org/10.1016/0021-9797(85)90400-X.

Gamsjäger, H., Bugajzki, J., Gajda, T., Lemire, R.J., Preis, W., 2005. Chemical Thermodynamics of Nickel. OECD Nuclear Energy Agency., p. 645

Giffaut, E., Grivé, M., Blanc, Ph, Viellard, Ph, Colás, E., Gailhanou, H., Gaboreau, S., Marty, N., Madé, B., Duro, L., 2014. Andra thermodynamic database for performance assessment: ThermoChimie. Appl. Geochem. 49, 225–236.

González-Siso, M.R., Gaona, X., Duro, L., Altmaier, M., Bruno, J., 2018. Thermodynamic model of Ni(II) solubility, hydrolysis and complex formation with ISA. Radiochim. Acta 106, 31–45. https://doi.org/10.1515/ract-2017-2762.

Grambow, B., López-García, M., Olmeda, J., Grivé, M., Marty, N.C.M., Grangeon, S., Claret, F., Lange, S., Deissmann, G., Klinkenberg, M., Bosbach, D., Bucur, C., Florea, I., Dobrin, R., Isaacs, M., Read, D., Kittnerová, J., Drtinová, B., Vopálka, D., Cevirim-Papaioannou, N., Ait-Mouheb, N., Gaona, X., Altmaier, M., Nedyalkova, L., Lothenbach, B., Tits, J., Landesman, C., Rasamimanana, S., Ribet, S., 2020. Retention and diffusion of radioactive and toxic species on cementitious systems: main outcome of the CEBAMA project. Appl. Geochem. 112 https://doi.org/10.1016/j.apgeochem.2019.104480.

Lothenbach, B., Nonat, A., 2015. Calcium silicate hydrates: solid and liquid phase composition. Cement Concr. Res. 78, 57–70. https://doi.org/10.1016/j.cemconres.2015.03.019.

Missana, T., García-Gutiérrez, M., Mingarro, M., Alonso, U., 2017. Analysis of barium retention mechanisms on calcium silicate hydrate phases. Cement Concr. Res. 93, 8–16. https://doi.org/10.1016/j.cemconres.2016.12.004.

Missana, T., García-Gutiérrez, M., Mingarro, M., Alonso, U., 2018. Comparison between cesium and sodium retention on calcium silicate hydrate (C–S–H) phases. Appl. Geochem. 98, 36–44. https://doi.org/10.1016/j.apgeochem.2018.09.007.

Missana, T., García-Gutiérrez, M., Mingarro, M., Alonso, U., 2019. Selenite retention and cation coadsorption effects under alkaline conditions generated by cementitious materials: the case of C-S-H phases. ACS Omega 4. https://doi.org/10.1021/acsomega.9b01637.

Nachtegaal, M., Sparks, D.L., 2002. Kinetics and mechanisms of nickel surface precipitation in multi-sorbent systems: a spectroscopic study. 17th world congr. Soil Sci. Bangkok, Thailand. August 14-21, 2002 1–10.

Noshita, K., Nishi, T., Yoshida, T., Fujihara, H., Saito, N., Tanaka, S., 2001. Categorization of cement hydrates by radionuclide sorption mechanism. Mater. Res. Soc. Symp. Proc. 663, 115–121. https://doi.org/10.1557/proc-663-115.

Ochs, M., Mallants, D., Wang, L., 2015. Radionuclide and metal sorption on cement and concrete. In: Topics in Safety, Risk, Reliability and Quality. Springer, Switzerland)-, ISBN 978-3-319-23651-3.

Payne, T.E., Brendler, V., Ochs, M., Baeyens, B., Brown, P.L., Davis, J.A., Ekberg, C., Kulik, D.A., Lutzenkirchen, J., Missana, T., Tachi, Y., Van Loon, L.R., Altmann, S., 2013. Guidelines for thermodynamic sorption modelling in the context of radioactive waste disposal. Environ. Model. Software 42, 143–156. https://doi.org/10.1016/j.envsoft.2013.01.002.

Pointeau, I., 2000. Etude mécanistique et modélisation de la retention de radionucléides par les phases de silicate de calcium des ciments hydrates. Thèse de l'Université de Reims-Champagne Ardennes, France. https://inis.iaea.org/collection/NCLCollectionStore/_Public/35/057/35057891.pdf.

Roosz, C., Gaboreau, S., Grangeon, S., Prêt, D., Montouillout, V., Maubec, N., Ory, S., Blanc, P., Vieillard, P., Henocq, P., 2016. Distribution of water in synthetic calcium silicate hydrates. Langmuir 32, 6794–6805. https://doi.org/10.1021/acs.langmuir.6b00878.

Scheckel, K.G., 1998. Assessment of Ni sorption mechanisms on soil mineral surfaces using time-resolved X-ray absorption fine structure (XAFS) spectroscopy. Mineral. Mag. 62A, 1330–1331. https://doi.org/10.1180/minmag.1998.62a.3.29.

Scheckel, K.G., Scheinost, A.C., Ford, R.G., Sparks, D.L., 2000. Stability of layered Ni hydroxide surface precipitates - a dissolution kinetics study. Geochem. Cosmochim. Acta 64, 2727–2735. https://doi.org/10.1016/S0016-7037(00)00385-9.

Scheidegger, A.M., Wieland, E., Scheinost, A.C., Dähn, R., Spieler, P., 2000. Spectroscopic evidence for the formation of layered Ni-Al double hydroxides in cement. Environ. Sci. Technol. 34, 4545–4548. https://doi.org/10.1021/es0000798.

Shi, Z., Peltier, E., Sparks, D.L., 2012. Kinetics of Ni sorption in soils: roles of soil organic matter and Ni precipitation. Environ. Sci. Technol. 46, 2212–2219. https://doi.org/10.1021/es202376c.

Tits, J., Wieland, E., Müller, C.J., Landesman, C., Bradbury, M.H., 2006. Strontium binding by calcium silicate hydrates. J. Colloid Interface Sci. 300, 78–87. https://doi.org/10.1016/j.jcis.2006.03.043.

Van der Lee, J., de Windt, L., 1999. CHESS tutorial and cookbook. Technical Report, LHM/RD/99/05.

Wieland, E., Van Loon, L., 2002. Cementitious near-field sorption data base for performance assessment of an ILW repository in Opalinus Clay, PSI Bericht Nr, 03-06. https://www.dora.lib4ri.ch/psi/islandora/object/psi%3A25335/datastream/PDF/Wieland-2003-Cementious_near-field_sorption_data_base-%28published_version%29.pdf.

Wieland, E., Tits, J., Ulrich, A., Bradbury, M.H., 2006. Experimental evidence for solubility limitation of the aqueous Ni(II) concentration and isotopic exchange of 63Ni in cementitious systems. Radiochim. Acta 94, 29–36. https://doi.org/10.1524/ract.2006.94.1.29.